J Mater Sci (2015) 50:4104–4114
DOI 10.1007/s10853-015-8966-4

Structures and properties of polyimide fibers containing ether units

Jingjing Chang[1] · Hongqing Niu[1] · Mengying Zhang[1] · Qiyan Ge[1] · Ya Li[1] · Dezhen Wu[1]

Received: 13 January 2015 / Accepted: 10 March 2015 / Published online: 17 March 2015

Abstract Copolyimide (co-PI) fibers containing 4,4′-oxydiphthalic anhydride (ODPA) moiety into the 3,3′,4,4′-biphenyltetracarboxylic dianhydride (BPDA)/*p*-phenylenediamine backbone were prepared via a two-step wet-spinning method. The processability and mechanical properties were improved significantly after the incorporation of ODPA, and the fibers exhibited an optimum tensile strength of 10.94 cN dtex^{-1} and modulus of 470.52 cN dtex^{-1} with elongation of 2.75 % at a BPDA/ODPA molar ratio of 7/3. Two-dimensional wide angle X-ray diffraction indicated that highly oriented structures and ordered molecular packing regions were formed in the fibers. Two-dimensional small angle X-ray scattering revealed that the incorporation of ODPA resulted in the reduction in radius, length, misorientation, and internal surface roughness of the microvoids in the fibers simultaneously, which was supposed to be mainly dominated for the drastically improved mechanical properties of PI fibers. Moreover, the co-PI fibers exhibited excellent thermal and thermal-oxidative stability, and the 5 % weight loss temperature was above 572 and 535 °C under nitrogen and air, respectively.

Introduction

High-performance aromatic polyimide (PI) fibers have been considered as one of the most promising engineering materials due to their excellent mechanical properties, thermal stability, and chemical resistance along with dielectric performance [1–3]. Currently, two major techniques including one-step method and two-step method are mainly used to prepare PI fibers [4–6]. As is well known, the earliest commercialized P84 fibers manufactured by Lenzing AG are derived from 3,3′,4,4′-benzophenonetetracarboxylic dianhydride (BTDA), 4,4′-diphenylmethane diisocyanate (MDI), and 2,4-tolylene diisocyanate (TDI) by the one-step method [7, 8]. In the one-step spinning process, PI fibers are produced directly from organ-soluble PIs synthesized via a polycondensation reaction of dianhydrides and diamines in toxic phenol solvents [4, 5, 9–12]. Due to the convenience in preparation of PI fibers, this method has been recognized as the most effective way to prepare PI fibers with excellent mechanical properties. Unfortunately, the selection of organ-soluble monomers and environment-friendly solvents has restricted the development of industrial production of PI fibers in the one-step method. Accordingly, the situation raises a critical demand for the researchers to turn their focus to the other technique two-step method, in which poly (amic acid) (PAA) fibers are obtained by extruding PAA solution into coagulation bath and subsequently converted into corresponding PI fibers through thermal or chemical imidization [13–15]. The first patent about PI fibers was published by DuPont company in 1960s, in which the PI fibers were prepared with pyromellitic dianhydride (PMDA), 4,4′-oxydianiline (ODA), and 4,4′-thiodianiline (TDA) in dimethylacetamide (DMAc) solvent by the two-step method [16]. By means of the extensive amount of potential monomers and solvents, the industrial level production of PI fibers is more likely to be realized in this method. Nevertheless, in the two-step wet-spinning method, the microvoids and other structural imperfection could generate through the dual-diffusion and imidization

✉ Dezhen Wu
wdz@mail.buct.edu.cn

[1] State Key Laboratory of Chemical Resource Engineering, College of Materials Science and Engineering, Beijing University of Chemical Technology, Beijing 100029, China

process, leading to a negative effect on the mechanical properties of PI fibers [17, 18]. To overcome the drawback, some modifications should be done in attempt to improve the mechanical properties.

Generally, the introduction of specific groups into the polymer backbone has been considered as a typical approach to modify the chemical structure of PI fibers, as outstanding properties of individual group could be integrated to form new high-performance polymers [19, 20]. So far, in order to improve mechanical properties of PI fibers, the monomers contain rigid aromatic heterocyclic units, such as 2-(4-aminophenyl)-6-amino-4(3*H*)-quinazolinone (AAQ), 2,5-bis(4-aminophenyl)-pyrimidine (2,5PRM), and 2-(4-aminophenyl)-5-aminobenzimidazole (BIA), are preferred to increase the rigidity of the polymer chain and introduce additional intermolecular associations [10, 21, 22]. For example, a series of PI fibers containing AAQ moiety were prepared by Niu et al. with the tensile strength and modulus up to 2.8 and 115.2 GPa, respectively. The incorporation of rigid-rod heterocyclic units containing both –NH– and =N– has enhanced the intermolecular associations via hydrogen bonding, which greatly affects the mechanical properties of PI fibers. Nevertheless, with the increased rigid units, it is difficult for the polymer chains to rearrange themselves to reduce the size of microvoids. On the contrary, the introduction of flexible units into rigid polymer backbone may provide opportunities to reduce the size of microvoids because of the increased flexibility of polymer chains, which posts a positive impact on the mechanical properties of PI fibers.

In the present work, a series of PI fibers were prepared by incorporating 4,4′-oxydiphthalic anhydride (ODPA) into 3,3′,4,4′-biphenyltetracarboxylic dianhydride (BPDA)/*p*-phenylenediamine (*p*-PDA) backbone. The BPDA/*p*-PDA system has been recognized to be promising to prepare high-performance PI fibers due to its low cost and high performance [23]. The processability and flexibility of PI fibers were improved significantly upon the incorporation of ODPA. Herein, we focus on the effect of the incorporation of ODPA on the properties of the co-PI fibers and also explore the evolution of molecular packing and morphology with the incorporated ODPA moiety, as introducing flexible units to improve mechanical properties of PI fibers through reducing the size of microvoids have remained to be explored.

Experimental

Materials

The monomers BPDA and ODPA were purchased from Shi Jiazhuang Hai Li Chemical Company and purified by sublimation prior to use. The monomer *p*-PDA was obtained from Shangyu Li Xing Chemical Company and purified by recrystallization. The solvent DMAc (analytical pure) was purchased from Tianjin Fu Chen Chemicals Reagent Factory and utilized after distillation. The deionized water used in the experiment was prepared by the Laboratory Water Purification System.

Preparation of the BPDA/ODPA/*p*-PDA (BOP) co-PI fibers

The co-PI fibers were prepared by the two-step wet-spinning method according to the following process. Take the polymerization of BOP-5 (the molar ratio of BPDA/ODPA is 5/5) PAA solution, for example, *p*-PDA (43.81 g) was first dispersed in 1000 ml DMAc solvent by stirring in the dried atmosphere. After the diamine was almost dissolved, the dianhydrides BPDA (59.59 g) and ODPA (62.83 g) were added in order. The solution was stirred for 5 h at low temperature to obtain a spinning solution containing 15 wt% solid content. The viscous solution, filtrated and degassed overnight before spinning, was extruded into coagulation bath through a spinneret (100 holes, 70 μm in diameter) to get as-spun PAA fibers under the pressure of nitrogen. The PAA fibers were then washed by deionized water to remove the residual solvent DMAc and dried in the oven with the temperature of 80 °C. Subsequently, the dried fibers were delivered into ovens at the temperature ranging from 280 to 500 °C with concomitant drawing on the spinning rollers. After the thermal imidization process, the mechanical properties of PI fibers were improved extensively. To make comparisons, the PI fibers with molar ratios of BPDA/ODPA varying from 10/0 to 5/5 were prepared under the same spinning condition. The reaction for the preparation of the co-PAA and co-PI fibers is listed in Scheme 1.

Characterization

The intrinsic viscosities of the co-PAA solutions were measured using a Germany SCHOTT 52510 Ubbelohde viscometer at 35 °C.

The apparent viscosities of the co-PAA solutions were performed by American Brookfield RVDVC viscometer at 30 °C. The samples were degassed prior to use. The relationship between viscosity of the fluid and shear rate can be evaluated by power law:

$$\eta = K\dot{\gamma}^n = Kc^n s^n, \quad (1)$$

where η is apparent viscosity of the fluid, $\dot{\gamma}$ is shear rate, s is shear speed of the rotator, c is constant that represents the coefficient of the rotator, and K and n are power law index.

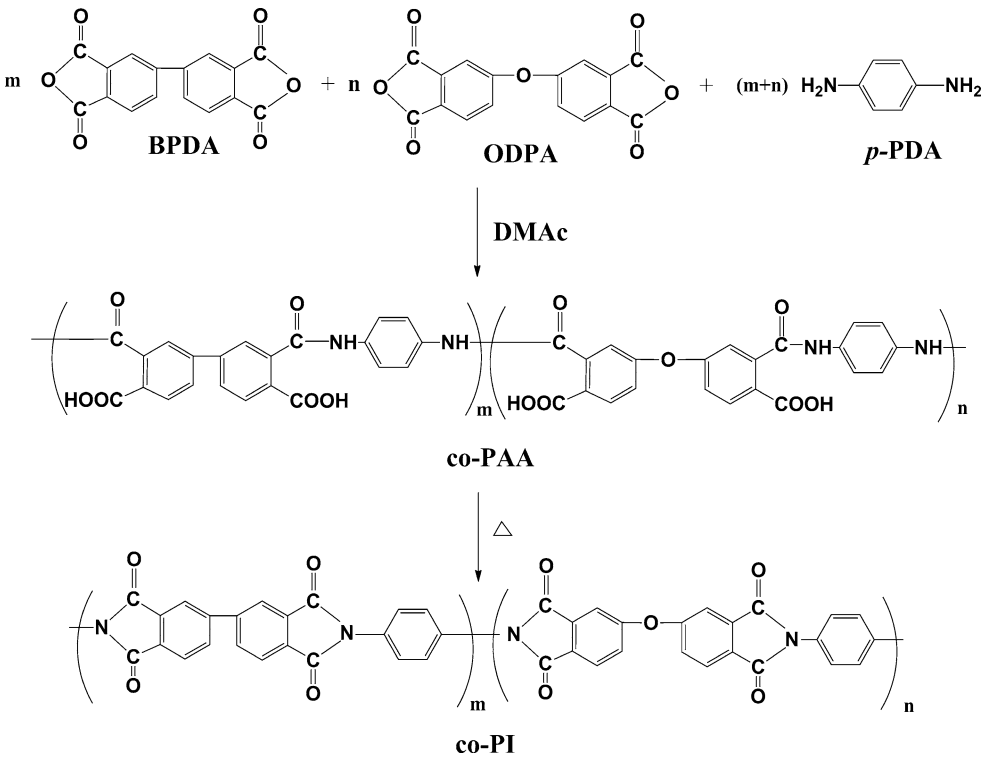

Scheme 1 The reaction for the preparation of the co-PAA and the co-PI fibers. m/n = 10/0, 9/1, 8/2, 7/3, 6/4, 5/5

Fourier transform infrared (FT-IR) measurement was carried out on Nexus 670 made by Nicolet Company with scanning wavenumber ranging from 4000 to 400 cm^{-1}.

The mechanical properties of PI fibers were measured using an YG001A-1 instrument with a gauge length and extension speed of 20 mm and 10 mm min^{-1}, respectively. For each type of fibers, at least 15 monofilaments were tested, and the average value was used as the representative.

Two-dimensional wide angle X-ray diffraction (2D WAXD) was performed on a Bruker D8 Discover diffractometer equipped with GADDS as a 2D detector. X-ray diffraction measurements were taken from reflection mode at room temperature using Ni-filtered Cu Kα ($\lambda = 0.154$ nm) radiation operated at 40 kV and 40 mA. The order degree X of macromolecule can be confirmed by the equation

$$X = \frac{U_0}{I_0} \times \frac{I_X}{U_X} \times 100\ \%, \tag{2}$$

where U_0 and U_X denote the backgrounds of the reference sample and experimental sample, and I_0 and I_X are integral intensities of diffraction lines of the reference sample and experimental sample, respectively. Moreover, the degree of molecular orientation can be calculated by integrating the corresponding intensity of azimuthal scans along the isolated and preferred crystalline plane [24]. The degree of molecular orientation in the fibers can be measured based on Herman's equation:

$$f = \left(3\langle\cos^2\phi\rangle - 1\right)/2, \tag{3}$$

where f is the degree of molecular orientation along the fiber axis direction and ϕ represents the angle between the fiber axis and c-axis crystal unit cell. The numerical values of the mean-square cosines in the equation above are determined by corrected intensity distribution $I(\phi)$ diffracted from the crystalline plane by Gaussian fitting following the equation

$$\langle\cos^2\phi\rangle = \frac{\int_0^{\pi/2} I(\phi)\sin\phi\cos^2\phi \mathrm{d}\phi}{\int_0^{\pi/2} I(\phi)\sin\phi \mathrm{d}\phi} \tag{4}$$

Two-dimensional small angle X-ray scattering (2D SAXS) was performed on NanoSTAR-U (BRUKER AXS INC) using an HI-STAR detector. The generator was operated at 40 kV and 650 μA with Cu Kα radiation. The distance between the sample and the detector was $L_{SD} = 1074$ mm. The effective scattering vector $\boldsymbol{q}$ ($\boldsymbol{q} = 4\pi\sin\theta/\lambda$, where 2θ is the scattering angle) at the distance ranges from 0.044 to 2.0 nm^{-1}.

As for wet-spinning process, the needle-like shape microvoids along the fiber axial direction can be characterized by SAXS. Therefore, the radius of microvoids can be described by Guinier functions as follows:

$$I(q) = I_0 \exp\left(\frac{-q^2R^2}{5}\right), \tag{5}$$

where R is the radius of the microvoids with circle cross-section and $I(q)$ is the scattering intensity in reciprocal. Through the Fankuchen successive tangent method, the average radius of microvoids can be calculated according to the equation

$$R = \sum R_i W_i (i = 1, 2, 3\ldots), \tag{6}$$

where R_i is the radius of different size of microvoids and W_i is the corresponding volume percentage of microvoids. Then the average fibril length L and misorientation B_ϕ are determined by the following equation proposed by Ruland:

$$s^2 B_{\text{obs}}^2 = \frac{1}{L^2} + s^2 B_\phi^2, \tag{7}$$

where B_{obs} is the angular spread of the data fitting by Gaussian–Gaussian function and s is the scattering vector ($s = 2\sin\theta/\lambda$). Furthermore, the fractal dimension D ($D = 6-\alpha$) is confirmed by the equation

$$I(q) \propto q^{-\alpha}, \tag{8}$$

where α is the constant that can be obtained from the experiment data.

Thermo gravimetric analysis (TGA) was performed with a TGA Q50 instrument at a heating rate of 10 °C min^{-1} from 50 to 900 °C under nitrogen and air.

Dynamic mechanical analysis (DMA) was performed on a DMA Q800 system with a load frequency of 1 Hz and heating rate of 5 °C min^{-1} at the temperature ranging from 50 to 450 °C.

Results and discussion

FT-IR spectra of the co-PI fibers

The chemical structures of PAA and PI fibers with different molar ratios of BPDA/ODPA are confirmed by FT-IR characterization as revealed in Fig. 1. Four characteristic absorption bands are observed at 1773, 1700, 1360, and 734 cm^{-1}, which are attributed to the C=O asymmetrical stretching of imide groups, C=O symmetrical stretching of imide groups, C–N stretching, and C=O bending of imide ring, respectively. Furthermore, the characteristic absorption bands of PAA fibers at 1660 cm^{-1} (amide-I band) and 1550 cm^{-1} (amide-II band) are not observed for co-PI fibers, indicating that the co-PI fibers have been successfully prepared by the two-step method after thermal imidization. In addition, the absorption band at 1264 cm^{-1} accounting for C–O–C stretching becomes much broader, and its intensity increases simultaneously with the increased ODPA content, suggesting that C–O–C groups have taken participate in the formation of chemical structures of PI fibers.

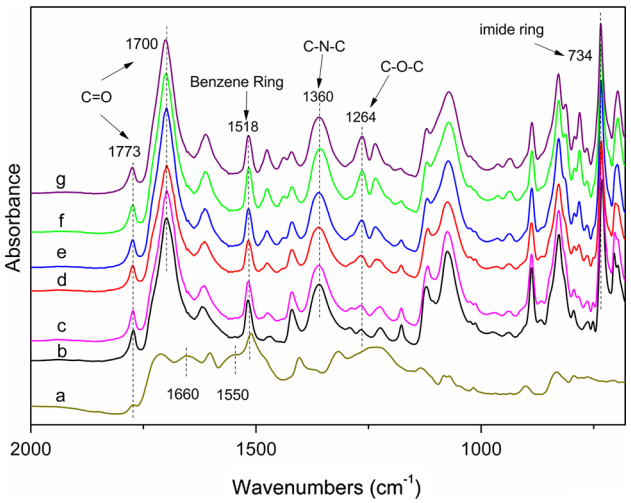

Fig. 1 FT-IR curves of the PAA and PI fibers with different molar ratios of BPDA/ODPA. *a* PAA-BP-0; *b* PI-BP-0; *c* PI-BOP-1; *d* PI-BOP-2; *e* PI-BOP-3; *f* PI-BOP-4; *g* PI-BOP-5

Mechanical properties of the co-PI fibers

The intrinsic viscosities of the co-PAA solutions and mechanical properties of the co-PI fibers are presented in Table 1. It can be observed that homo-PI (BP-0) fibers exhibit the tensile strength of 7.41 cN dtex^{-1}, modulus of 349.92 cN dtex^{-1}, and elongation of 1.12 %. Apparently, the tensile strength and modulus were improved significantly upon the incorporation of ODPA, ranging from 8.48 and 10.94 cN dtex^{-1} to 361.78 and 470.52 cN dtex^{-1}, respectively. The BOP-3 fibers, which possess a BPDA/ODPA molar ratio of 7/3, own the optimum mechanical properties with the tensile strength and modulus of 10.94 and 470.52 cN dtex^{-1}, respectively. It should be noticed that the mechanical properties of PI fibers were improved before the ODPA content reaches 30 %, and further increasing ODPA content leads to the slightly decrease in mechanical properties of PI fibers. The possible reason for the extensive improvement is inferred as follows. It is well known that the mechanical properties of PI fibers are closely dependent on the intrinsic viscosities, intermolecular interaction, and rigidity of polymer backbone, molecular packing, and structural defects [24–27]. Currently, the intrinsic viscosities of PAA solutions range from 1.80 to 2.32 dL g^{-1} without the ordered regularity, implying that the enhancement in mechanical properties is not mainly affected by the intrinsic viscosity. Moreover, the ether bonds have not introduced any intermolecular associations in the formation of chemical structures of PI fibers, giving no evidence in improving mechanical properties of PI fibers. On the other hand, with increased flexible units, the efficiently improved flexibility of PI fibers provides opportunities for the rearrangement of the polymer chains

Table 1 The intrinsic viscosities of the synthesized co-PAA solutions with different molar ratios of BPDA/ODPA and the mechanical properties of the corresponding co-PI fibers

PI fibers	Molar ratio of BPDA/ODPA	Intrinsic viscosity (dL/g)	Strength (cN/dtex)	Modulus (cN/dtex)	Elongation (%)
BP-0	10/0	2.32	7.41	349.92	1.12
BOP-1	9/1	1.98	8.48	400.49	2.40
BOP-2	8/2	1.80	9.27	428.65	2.47
BOP-3	7/3	2.17	10.94	470.52	2.75
BOP-4	6/4	2.12	10.03	411.63	2.59
BOP-5	5/5	1.92	8.62	361.78	2.58

under large deformation as well as for the reduction of the size of microvoids. Thus, it is speculated that the variation of the molecular packing and structural defects has made great contributions to the improved mechanical properties of PI fibers.

Molecular packing of the co-PI fibers

For aromatic PI fibers, the crystallinity and molecular orientation are two crucial subjects that determine the final performance of PI fibers during imidization process. In order to investigate the effect of these basic structure parameters on the performance of PI fibers, the 2D WAXD patterns of PI fibers with different molar ratios of BPDA/ODPA are obtained as shown in Fig. 2. Along the meridian direction, all the fibers exhibit clear diffraction streaks, revealing a high orientation in the fiber axial direction. Along the equator direction, the obscure amorphous halos indicate the fibers consisting of poor ordered lateral packing structures of PI chains. Moreover, there is no evidence of diffractions in the quadrants, demonstrating that the prepared co-PI fibers do not exhibit well-defined 3D crystalline structures.

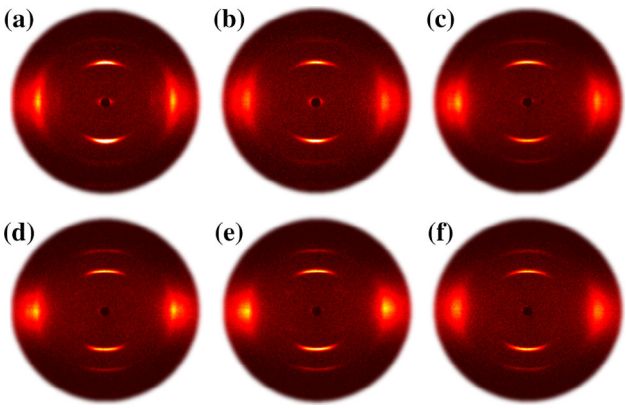

Fig. 2 2D WAXD patterns of the co-PI fibers with different molar ratios of BPDA/ODPA. **a** BP-0; **b** BOP-1; **c** BOP-2; **d** BOP-3; **e** BOP-4; **f** BOP-5

For details, the WAXD patterns profiles along the meridian and equator directions of the co-PI fibers are displayed in Fig. 3a and b, respectively. As observed in Fig. 3a, three diffraction peaks at 11.1° ($d = 0.796$ nm), 17.4° ($d = 0.509$ nm), and 23.1° ($d = 0.385$ nm) appear in homo-PI fibers. On the basis of our previous work, the lowest energy conformation for BPDA/*p*-PDA units was obtained as a repeat length of 1.587 nm by computer simulation [10]. The value is close to the twice of the observed data at $2\theta = 11.1°$ ($0.796 \times 2 = 1.592$ nm), and the diffraction streak is set to be the (002) plane. Therefore, the peak at $2\theta = 17.4$ and 23.1° can be assigned to be (003) and (004), respectively. With the increased ODPA content, dramatic changes occur in the WAXD patterns. The peak at 11.1° finally shifts to 11.0° after the incorporation of ODPA, resulting in the slightly increased chain repeat length along the fiber axial direction, since some BPDA/*p*-PDA units have been replaced by larger ODPA/*p*-PDA units. In the meantime, the intensity of the peak at 17.4° increases initially and then decreases at a BPDA/ODPA molar ratio of 7/3. Moreover, the peak at 23.1° becomes much diffuse and completely disappears for BOP-5 fibers.

On the equator direction as revealed in Fig. 3b, a series of broad diffraction peaks around 18.1° are identified, which are 18.1, 18.4, 18.6, 18.4, 18.5, and 18.7°, corresponding to BP-0, BOP-1, BOP-2, BOP-3, BOP-4, and BOP-5 fibers, respectively, giving evidence of decreased *d*-spacing with increasing ODPA content. Meanwhile, the order degree of macromolecule is calculated to be 2.19 U_0/I_0, 1.99 U_0/I_0, 1.97 U_0/I_0, 2.13 U_0/I_0, 2.06 U_0/I_0, and 1.98 U_0/I_0 based on Eq. (2) [28]. It should be noted that the *d*-spacing and order degree of the co-PI fibers exhibit the similar trend, indicating that the high-order degree of macromolecule could result in the loose packing structures. Furthermore, the peaks become much broader and diffuse after the introduction of ODPA, revealing the gradually decreased order degree of lateral packing structures.

In addition, the degree of molecular orientation along the fiber axial direction was also studied by WAXD. The degree of molecular orientation of (002) plane can be

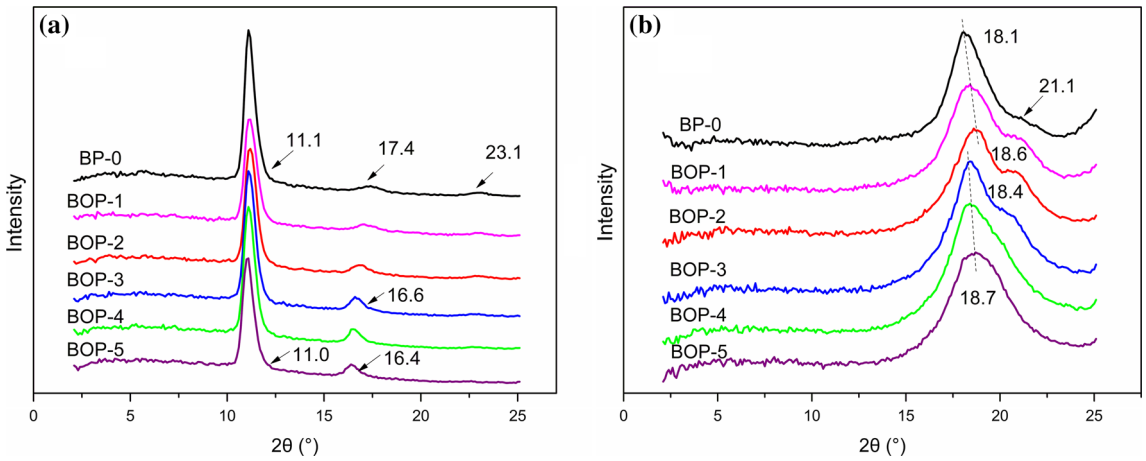

Fig. 3 WAXD intensity profiles of the co-PI fibers with different molar ratios of BPDA/ODPA. **a** meridian direction; **b** equator direction

Table 2 The calculated molecular orientation of the co-PI fibers

PI fibers	BP-0	BOP-1	BOP-2	BOP-3	BOP-4	BOP-5
Degree of orientation	0.87	0.86	0.85	0.80	0.83	0.84

calculated according to Eq. (3) and (4). According to the results in Table 2, the degree of orientation decreases after the introduction of ODPA and reaches the lowest value for BOP-3 fibers. However, with further increased ODPA content, the degree of orientation starts to increase on the opposite. For PI fibers, there is a certain degree of molecular orientation during the spinning and drawing process, which may affect the properties of PI fibers. In the present work, the chains have endured almost the same degree of orientation with consistent draw ratio in drawing process, and as a consequence, the final molecular orientation of PI fibers is determined during the spinning process.

The schematic diagram of the velocity gradient of PAA solution and corresponding macromolecule structure behavior in wet-spinning process is depicted in Fig. 4. Due to the shear flow in the spinning cylinder, the macromolecules tend to stretch out to flow more freely, which is called as disentanglement. After extruding PAA solution out the spinneret, the macromolecules gradually entangle to form random coils to recovery elastic deformation in response to the loss of shear stress, which is known as Barus effect. With concomitant drawing on the spinning rollers, the macromolecules have oriented along the drawing direction. Meanwhile, PAA fibers are gradually freezed through the dual-diffusion process. However, the series of co-PAA solutions exhibit various elastic recovery capabilities, which are greatly dependent on the sensibilities of viscosities to the shear speed and subsequently influence the molecular orientation in the spinning process. Therefore, the relationship between apparent viscosities $[\eta]$ of the co-PAA solutions and shear speed s is discussed to observe the dependence of viscosities of the co-PAA solutions on the shear speed as illustrated in Fig. 5a and b. The curves indicate that the co-PAA solutions behave as typical non-Newtonian fluids, and the viscosities decrease greatly at a low shear speed, giving evidence of strong dependence on the shear speed. In addition, in order to further investigate the dependence variation of the co-PAA solutions on shear speed, the $\ln [\eta]$ versus $\ln s$ plots of the co-PAA solutions are present in Fig. 5b based on Eq. (1). The slopes of fitting curves are found to be −0.71, −0.62, −0.38, −0.37, −0.45, and −0.66, corresponding to BP-0, BOP-1, BOP-2, BOP-3, BOP-4 and BOP-5 co-PAA solution, respectively. Generally, it is suggested that the high value in slope results in relatively poor dependence of viscosity on shear speed and slow elastic deformation recovery after extruding PAA solution out the spinneret. Herein, the BOP-3 PAA solution exhibits the highest value of slope in the series of co-PAA solutions and keeps the most oriented chains with the highest intermolecular interaction. Meanwhile, the increased physical entanglement points will be generated after the introduction of ODPA due to the improved flexibility of polymer chains. It should be noted that both the increased intermolecular interaction and entanglement points will not facilitate the further orientation by drawing. As a consequence, both the two sides result in the lowest degree of molecular orientation for BOP-3 fibers. The result is in agreement with the calculated degree of molecular orientation. In conclusion, it is reasonable to believe that the improvement in mechanical properties is not mainly dominated by molecular orientation in the present work.

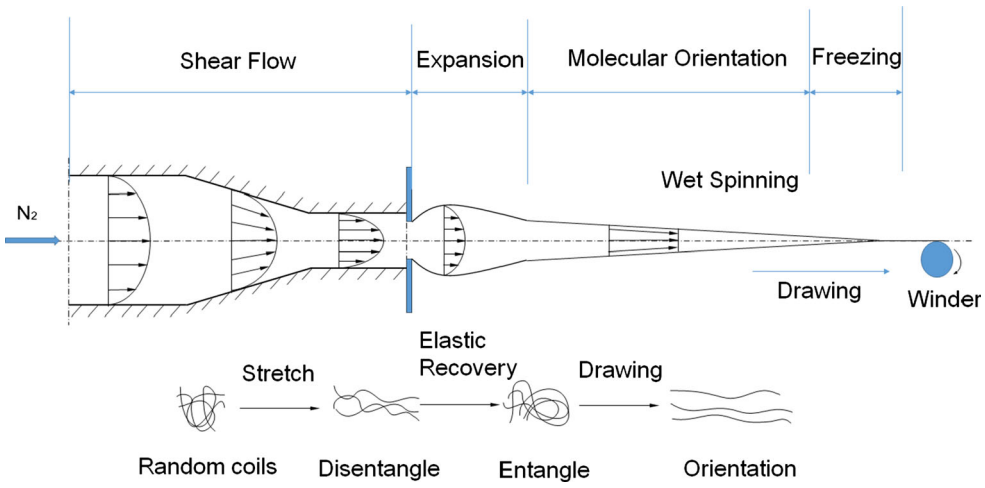

Fig. 4 Schematic diagram of the velocity gradient of PAA solution and corresponding macromolecule structure behavior in wet spinning

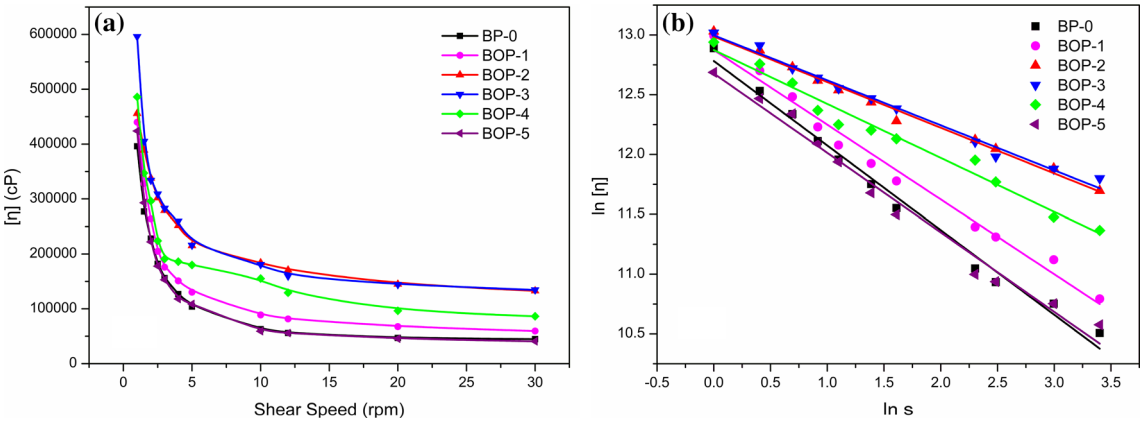

Fig. 5 **a** The viscosities of the co-PAA solutions with different shear speed; **b** The ln $[\eta]$ versus ln s plots of the co-PAA solutions

Morphologies of the co-PI fibers

In wet spinning, some defects such as microvoids could be formed during the dual-diffusion and thermal imidization process due to the removal of micromolecules. In this section, the morphological evolution of BOP fibers after thermal imidization was characterized by 2D SAXS. As the scattering from microvoids typically accounts for the most overall scattering in semicrystalline polymers [29, 30], SAXS has become an ideal tool to investigate the nanoscale structural change of PI fibers. With regards to PI fibers, the microvoids were distributed approximately parallel to the fiber axis. Upon the introduction of ODPA content, the parameters such as the average radius R, length L, and misorientation B_ϕ of microvoids will vary accompanied with the evolution of aggregation state in the fibers.

As demonstrated in Fig. 6, the 2D and 1D SAXS patterns along the meridian direction of the co-PI fibers with different molar ratios of BPDA/ODPA are obtained. All the scattering patterns show intense and elongated streaks near the beamstop along the fiber axial direction, which reflects the oriented needle-like structure of microvoids aligned parallel to the fiber axis. Moreover, the scattering intensity of BOP fibers gradually decreases along with the increased scattering vector $\boldsymbol{q}$, indicating the existence of nanoscale structure in the fibers. In order to determine the size of microvoids, the Guinier functions are introduced as displayed in Eq. (5) [31, 32]. Taking the BOP-3 fibers as illustrated in Fig. 7, for example, the radius R_i ($i = 1, 2, 3$) and corresponding volume percentage W_i ($i = 1, 2, 3$) to different size of microvoids can be confirmed by Fankuchen successive tangent method. The average radius R of microvoids can be calculated according to Eq. (6), which are listed in Table 3 [33]. Obviously, the radius of the microvoids decreases along with increased ODPA content until the molar ratio of BPDA/ODPA reaches 7/3 and then increases with further introduction of ODPA. It is still related to the rheological property of co-PAA solutions. Due to the slowest elastic recovery deformation of BOP-3 PAA solution, the least entanglement points are formed in the macromolecule chains during the

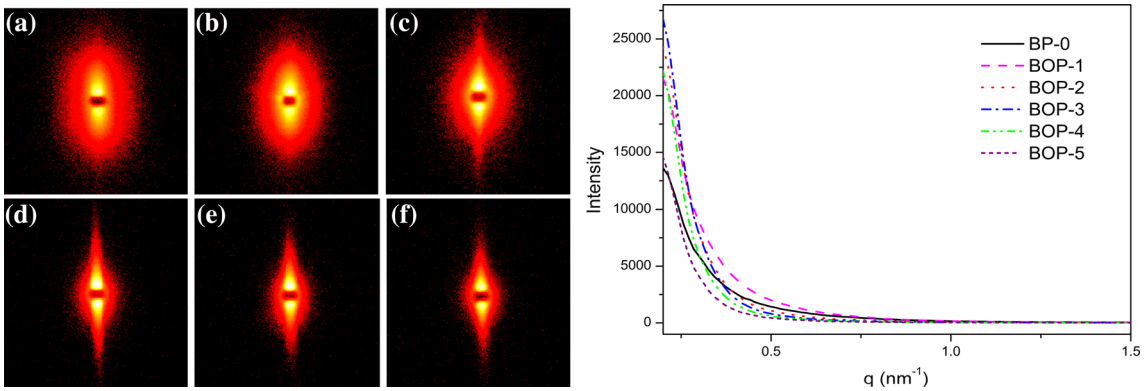

Fig. 6 The 2D and 1D SAXS patterns of the co-PI fibers with different molar ratios of BPDA/ODPA. **a** BP-0; **b** BOP-1; **c** BOP-2; **d** BOP-3; **e** BOP-4; **f** BOP-5

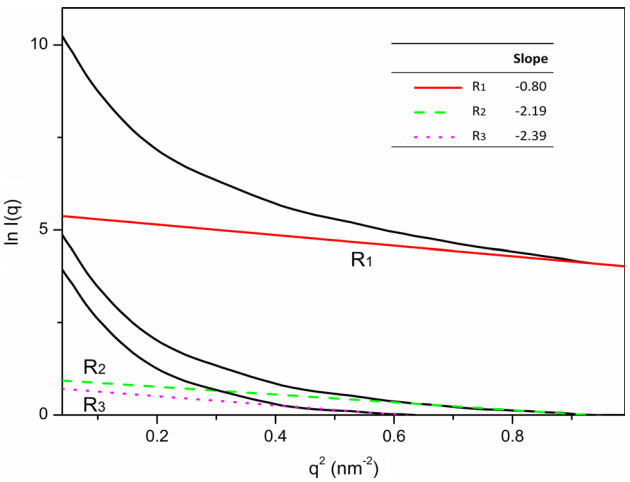

Fig. 7 Guinier plot of the scattered intensities of BOP-3 fibers along the meridian direction by Fankuchen successive tangent method

spinning process, which provides the segmental motion capability for macromolecule chains to reduce the size of microvoids during the dual-diffusion process.

Moreover, both the size distribution and misorientation of microvoids have contributed to the streak profile as reported by Ran et al. [34]. The average fibril length L and misorientation B_ϕ could be analyzed with the equation expressed as Eq. (7) proposed by Ruland [35]. The intensity profiles corresponding to azimuthal scans extracted at different scattering vectors and Ruland plot for the BP-0 fibers are shown in Fig. 8a and b, respectively. The length L is obtained from the intercept of the $s^2B^2_{\text{obs}}$ versus s^2 plot and misorientation B_ϕ from the slope of the plot, which are listed in Table 3 as well. Analogously, the L and B_ϕ decrease after the incorporation of ODPA, and the values increase slightly when the ODPA content is over 30 %. It can be concluded that the microvoids tend to decrease in the size and distribute parallel to the fiber axial direction upon the introduction of ODPA, leading to the improved mechanical properties of PI fibers.

Furthermore, the fractal dimension D, focused on the internal surface roughness of microvoids, is also a crucial factor that affects the mechanical properties of PI fibers. Followed by the equation given in Eq. (8), the slope -α can be inferred from the ln $I(q)$ versus ln q plot, and subsequently the fractal dimension D can be obtained as displayed in Fig. 9. Herein, the results give an evidence of decreasing tendency of D, which correlates with that of the mechanical properties of PI fibers. Basically, the higher the D value, the stronger the internal surface roughness of microvoids [23]. In addition, the rough surface of microvoids could easily concentrate stress and thus leads to the generation of defect structures, which restricts the improvement in mechanical properties. In conclusion, the reduced internal surface roughness of microvoids has well confirmed the improvement in mechanical properties of PI fibers.

Table 3 The parameters of microvoids of the co-PI fibers prepared with different molar ratios of BPDA/ODPA

PI fibers	R_i						R (nm)	L (nm)	B_ϕ (°)
	R_1 (nm)	W_1	R_2 (nm)	W_2	R_3 (nm)	W_3			
BP-0	1.29	1.00	0.94	0.21	1.14	0.06	1.56	119.61	31.68
BOP-1	1.26	1.00	0.79	0.25	0.62	0.15	1.55	106.02	27.60
BOP-2	1.08	1.00	0.55	0.30	0.88	0.14	1.37	97.78	22.12
BOP-3	0.76	1.00	1.26	0.08	1.33	0.03	0.90	97.66	15.21
BOP-4	0.92	1.00	1.05	0.13	1.05	0.11	1.16	98.15	16.73
BOP-5	0.94	1.00	0.97	0.19	1.32	0.05	1.19	99.21	19.42

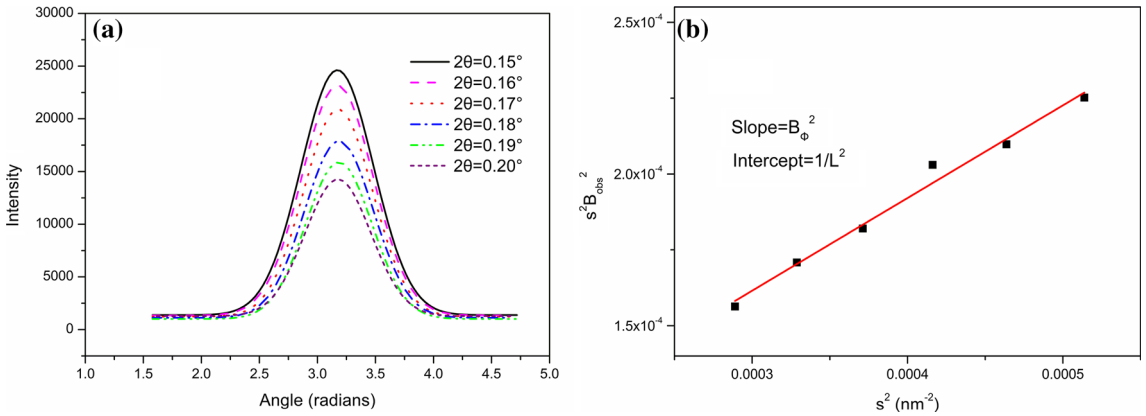

Fig. 8 **a** Intensity profiles corresponding to azimuthal scans at different scattering vectors of the BP-0 fibers; **b** Ruland plot of the BP-0 fibers

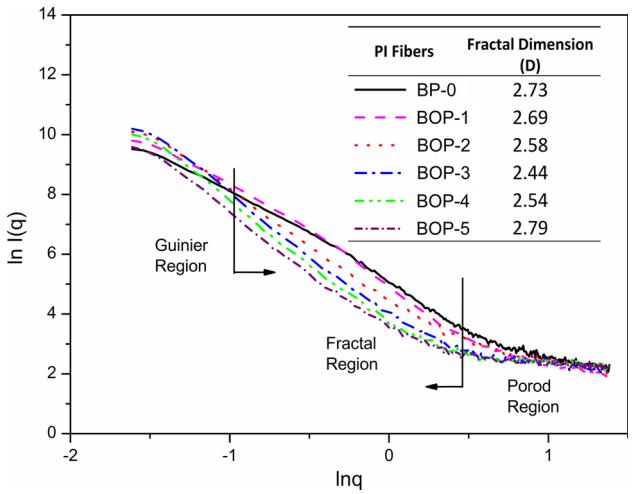

Fig. 9 Fractal features of the co-PI fibers with different molar ratios of BPDA/ODPA

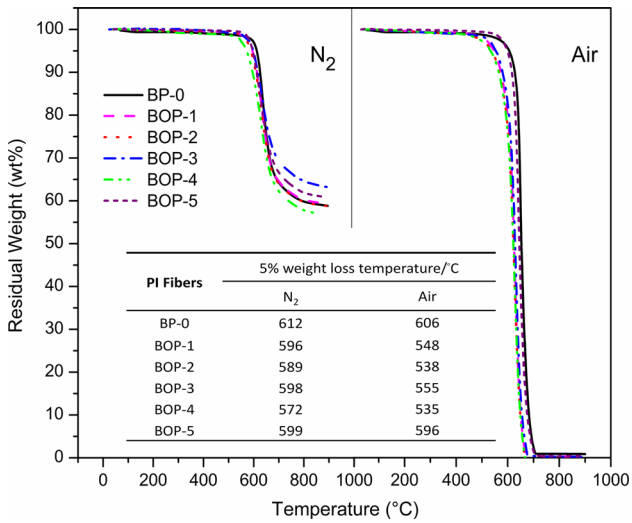

Fig. 10 TGA curves of the co-PI fibers under nitrogen and air

Thermo gravimetric analysis of the co-PI fibers

Figure 10 illustrates the thermal stability of the co-PI fibers heated from 50 to 900 °C at a heating rate of 10 °C min^{-1} in nitrogen and air. The homo-PI fiber exhibits 5 % weight loss temperature (T_{d5}) at 612 and 606 °C in nitrogen and air, respectively. After the introduction of ODPA, the value of T_{d5} ranges from 572 to 599 °C in nitrogen and 535 to 596 °C in air, indicating the reduction in thermal stability with the increased ODPA content. Nevertheless, the T_{d5} moves to high value at a BPDA/ODPA molar ratio of 5/5 in both nitrogen and air atmosphere, which can be inferred through WAXD patterns of the co-PI fibers. With regards to BOP-5 fibers, the broad peak along the equator direction shifts to high value at 18.7°, indicating the reduction in *d*-spacing in the fibers. Thus, the compact lateral stacking structures are conducive to improve the thermal stability of PI fibers. In conclusion, the introduction of ODPA leads to the reduction in the thermal stability of PI fibers because of the decreased rigidity of polymer backbone. Ultimately, all the fibers exhibit excellent thermal stabilities with the 5 % weight loss temperature above 572 and 535 °C under nitrogen and air, respectively.

Dynamic mechanical analysis of the co-PI fibers

Figure 11 demonstrates the DMA curves of the co-PI fibers evaluated at a heating rate of 5 °C min^{-1} from 50 to 450 °C in nitrogen atmosphere. Two series of peaks are identified in the curves, in which the higher ones are α relaxations corresponding to the glass transition temperature (T_g) of the PI fibers, and the other ones are β relaxations representing sub-glass transition of the PI fibers. For α relaxation, with increased ODPA content, the value of T_g of the co-PI fibers exhibits a pronounced decreased tendency due to the increased flexibility of the

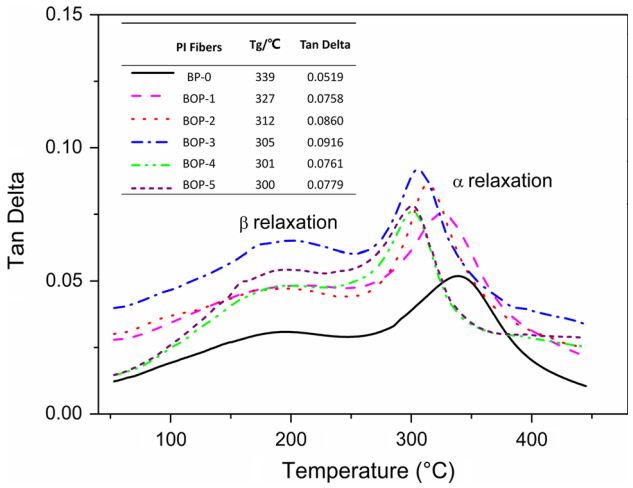

Fig. 11 DMA curves of the co-PI fibers with different molar ratios of BPDA/ODPA

polymer chains. Meanwhile, the value of tan delta exhibits a clear increased tendency induced by the incremental energy consumption of segmental motion of the chains. It is worth noticing that the value of tan delta shows a slightly decrease when the ODPA content is over 40 %, which can be explained by the contributions mentioned as follows. First, although the flexibility has been enhanced upon the introduction of ODPA, the improvement in the flexibility for BOP-4 and BOP-5 fibers is not obvious as can be observed from the data of T_g. On the other hand, the impact lateral structures have been gradually formed (from WAXD patterns), and thus the improved packing structures have led to the restricted segmental motion of the chains. As a consequence, the two opposite effects have resulted in the slightly decreased intensity of α relaxation. In addition, the appearance of the β relaxation was related to the conformation change of BPDA (*cis* to *trans*), as the bonds that connect two phenol rings tend to rotate to form planar conformation to set the lowest energy conformation [24, 36].

Conclusion

A series of high-performance PI fibers containing ODPA moiety have been prepared by a two-step wet-spinning method. The mechanical properties of the co-PI fibers were evidently improved by incorporating flexible monomer ODPA into rigid BPDA/*p*-PDA backbone. The optimum mechanical properties of the co-PI fibers were realized when the BPDA/ODPA molar ratio was 7/3, with the tensile strength and modulus of 10.94 cN dtex^{-1} and 470.52 cN dtex^{-1}, respectively. Moreover, the evolution of oriented molecular packing and morphologies was characterized by 2D WAXD and 2D SAXS, respectively. Highly oriented structures along the fiber axial direction were observed in the series of PI fibers, and a degree of molecular orientation of 0.80 was obtained for optimum BOP-3 fibers. Under the same external conditions, the molecular orientation was mainly dominated during spinning process, and the high degree of molecular orientation was obtained for the PAA solution which possessed strong dependence of viscosity on shear speed. In addition, the average radius, length, misorientation, and internal surface roughness of microvoids were found to decrease with increased ODPA content until the molar ratio of BPDA/ODPA was over 7/3, which should be responsible for the improved mechanical properties of PI fibers. In conclusion, all the fibers exhibited excellent thermal and thermal-oxidative stability, although the introduction of ODPA led to the slightly reduction in the thermal properties. Consequently, we developed a new approach in preparing high-performance PI fibers via the two-step wet-spinning method.

Acknowledgements The authors greatly thank the financial support from the National Natural Science Foundation of China (No. 51373008) and Beijing Key New Materials Research and Application Project (No. Z141100004214005).

References

1. Kricheldorf HR (1999) Progress in polymer chemistry, advance in polymer science. Springer, Berlin
2. Hasegawa M, Horie K (2001) Photophysics, photochemistry, and optical properties of polyimides. Prog Polym Sci 26:259–335
3. Luo LB, Pang YW, Jiang X, Liu XY (2012) Preparation and characterization of novel polyimide films containing amide groups. J Polym Res 19:9783–9789
4. Eashoo M, Shen DX, Wu ZQ, Harris FW, Cheng SZD (1993) High-performance aromatic polyimide fibres: 2. Thermal mechanical and dynamic properties. Polymer 34:3209–3215
5. Cheng SZD, Wu ZQ, Eashoo M, Hsu SLC, Harris FW (1991) A high-performance aromatic polyimide fibre: 1. Structure, properties and mechanical-history dependence. Polymer 32:1803–1810
6. Zhang QH, Dai M, Ding MX, Chen DJ, Gao LX (2004) Mechanical properties of BPDA-ODA polyimide fibers. Eur Polym J 40:2487–2493
7. Qiao XY, Chung TS, Pramoda KP (2005) Fabrication and characterization of BTDA-TDI/MDI (P84) co-polyimide membranes for the pervaporation dehydration of isopropanol. J Membr Sci 264:176–189
8. Xiang HB, Huang Z, Liu LQ, Yu JR (2011) Structure and properties of polyimide (BTDA-TDI/MDI co-polyimide) fibers obtained by wet-spinning. Macromol Res 19:645–653
9. Li FM, Ge JJ, Honigfort PS, Fang S, Chen JC, Harris FW (1990) Dianhydride architectural effects on the relaxation behaviors and thermal and optical properties of organo-soluble aromatic polyimide films. Polymer 40:4987–5002
10. Niu HQ, Huang MJ, Qi SL, Han EL, Tian GF, Wang XD, Wu DZ (2013) High-performance copolyimide fibers containing quinazolinone moiety: preparation, structure and properties. Polymer 54:1700–1708

11. Xu Y, Wang SH, Li ZT, Xu Q, Zhang QH (2013) Polyimide fibers prepared by dry-spinning process: imidization degree and mechanical properties. J Mater Sci 48:7863–7868. doi:10.1007/s10853-013-7310-0
12. Dong J, Yin CQ, Luo WQ, Zhang QH (2013) Synthesis of organ-soluble copolyimides by one-step polymerization and fabrication of high performance fibers. J Mater Sci 48:7594–7602. doi:10.1007/s10853-013-7576-2
13. Chen D, Liu TX, Zhou XP, Hou HQ (2009) Electrospinning fabrication of high strength and toughness polyimide nanofiber membranes containing multiwalled carbon nanotubes. J Phys Chem B 113:9741–9748
14. Dorogy JWE, Clair AKS (1991) Wet spinning of solid polyamic acid fibers. J Appl Polym Sci 43:501–519
15. Dorogy JWE, Clair AKS (1993) Fibers from a soluble, fluorinated polyimide. J Appl Polym Sci 49:501–510
16. Irwin RS (1968) Formation of polypyromellitimide filaments. US Patent 3,415,782
17. Kaneda T, Katsura T, Nakagawa K, Makino H, Horio M (1986) High-strength-high-modulus polyimide fibers I. One-step synthesis of spinnable polyimides. J Appl Polym Sci 32:3133–3149
18. Kaneda T, Katsura T, Nakagawa K, Makino H, Horio M (1986) High-strength high-modulus polyimide fibers II. Spinning and properties of fibers. J Appl Polym Sci 32:3151–3176
19. Russo S, Bianchi E, Mariani A, Mendichi R (2000) A study on the *N*-allylation reaction of aromatic polyamides. 1. Poly(p-phenylene terephthalamide). Macromolecules 33:4390–4397
20. Lammers M, Klop EA, Northolt MG, Sikkema DJ (1998) Mechanical properties and structural transitions in the new rigid-rod polymer fibre PIPD ('M5') during the manufacturing process. Polymer 39:5999–6005
21. Sukhanova TE, Baklagina YG, Kudryavtsev VV, Maricheva TA, Lednicky F (1999) Morphology, deformation and failure behaviour of homo- and copolyimide fibres: 1. Fibres from 4,4′-oxybis(phthalic anhydride) (DPhO) and *p*-phenylenediamine (PPh) or/and 2,5-bis(4-aminophenyl)-pyrimidine (2,5PRM). Polymer 40:6265–6276
22. Dong J, Yin CQ, Zhang ZX, Wang XY, Li HB, Zhang QH (2014) Hydrogen-bonding interactions and molecular packing in polyimide fibers containing benzimidazole units. Macromol Mater Eng 299:1170–1179
23. Huang SB, Jiang ZY, Ma XY, Qiu XP, Men YF, Gao LX, Ding MX (2013) Properties, morphology and structure of BPDA/PPD/ODA polyimide fibers. Plast Rubber Compos 42:407–415
24. Hsiao SH, Chen YJ (2002) Structure-property study of polyimides derived from PMDA and BPDA dianhydrides with structurally different diamines. Eur Polym J 38:815–828
25. Hasegawa M, Sensui N, Shindo Y, Yokota R (1999) Structure and properties of novel asymmetric biphenyl type polyimides. Homo- and copolymers and blends. Macromolecules 32:387–396
26. Hasegawa M, Sensui N, Shindo Y, Yokota R (1999) Improvement of thermoplasticity for s-BPDA/PDA by copolymerization and blend with novel asymmetric BPDA-based polyimides. J Polym Sci Part B 37:2499–2511
27. Liu JP, Zhang QH, Xia QM, Dong J, Xu Q (2012) Synthesis, characterization and properties of polyimides derived from a symmetrical diamine containing bis-benzimidazole rings. Polym Degrad Stabil 97:987–994
28. Liu XY, Guo LH, Gu Y (2005) A novel aromatic polyimide with rigid biphenyl side-groups: formation and evolution of structures in thermoreversible gel. Polymer 46:11949–11957
29. Grubb DT, Prasad K (1992) High-modulus polyethylene fiber structure as shown by x-ray diffraction. Macromolecules 25:4575–4582
30. Wu J, Schultz JM, Ye FJ, Hsiao BS, Chu BJ (2000) In-situ simultaneous synchrotron small- and wide-angle X-ray scattering measurement of poly(vinylidene fluoride) fibers under deformation. Macromolecules 33:1765–1777
31. Jiang GS, Huang WF, Li L, Wang X, Pang FJ, Zhang YM, Wang HP (2012) Structure and properties of regenerated cellulose fibers from different technology processes. Carbohydr Polym 87:2012–2018
32. Jiang GS, Yuan Y, Wang B, Yin X, Mukuze KS, Huang WF (2012) Analysis of regenerated cellulose fibers with ionic liquids as a solvent as spinning speed is increased. Cellulose 19:1075–1083
33. Wang W, Chen X (2008) In situ SAXS study on size changes of platinum nanoparticles with temperature. Eur Phys J Part B 65:57–64
34. Ran S, Fang D, Zong X, Hsiao B, Chu B, Cunniff PM (2001) Structural changes during deformation of Kevlar fibers via on-line synchrotron SAXS/WAXD techniques. Polymer 42:1601–1612
35. Ruland W (1969) Small-angle scattering studies on carbonized cellulose fibers. J Polym Sci Part C 1:143–151
36. Eashoo M, Wu ZQ, Zhang AQ, Shen DX, Harris FW, Cheng SZD (1994) High performance aromatic polyimide fibers, 3. A polyimide synthesized from 3,3′,4,4′-biphenyltetracarboxylic dianhydride and 2,2′-dimethyl-4,4′-diaminobiphenyl. Macromol Chem Phys 195:2207–2225